Morphing Activity between Structurally Similar Enzymes: From Heme-Free Bromoperoxidase to Lipase

ARTICLE *in* BIOCHEMISTRY · NOVEMBER 2009

Impact Factor: 3.02 · DOI: 10.1021/bi9014727 · Source: PubMed

6 AUTHORS, INCLUDING:

Zhen Cai
Chinese Academy of Sciences
24 PUBLICATIONS **107** CITATIONS
SEE PROFILE

Wei Wu
Chinese Academy of Sciences
7 PUBLICATIONS **90** CITATIONS
SEE PROFILE

Juergen Pleiss
Universität Stuttgart
174 PUBLICATIONS **3,755** CITATIONS
SEE PROFILE

11496 *Biochemistry* **2009,** *48,* 11496–11504
DOI: 10.1021/bi9014727

BIOCHEMISTRY
including biophysical chemistry & molecular biology
Article

Morphing Activity between Structurally Similar Enzymes: From Heme-Free Bromoperoxidase to Lipase[†]

Bo Chen,[‡] Zhen Cai,[‡,∥] Wei Wu,[‡] Yunlong Huang,[‡] Juergen Pleiss,*[,§] and Zhanglin Lin*[,‡]

[‡]*Department of Chemical Engineering, Tsinghua University, Tsinghua Garden Road 1, 100084 Beijing, China, and* [§]*Institute of Technical Biochemistry, University of Stuttgart, Allmandring 31, 70569 Stuttgart, Germany.* [∥]*Present address: Institute of Microbiology, Chinese Academy of Sciences, Beichen West Road 1, 100101 Beijing, China.*

Received August 22, 2009; Revised Manuscript Received October 30, 2009

ABSTRACT: In this study, to explore the plasticity of the α/β-hydrolase fold family, we converted bromoperoxidase A2 (BPO-A2) from *Streptomyces aureofaciens* to a lipase by structure comparison with lipase A (LipA) from *Bacillus subtilis*. These two enzymes have similar structures (2.1 Å rmsd) and a very low level of sequence identity (∼18%). A variant BL1 was constructed by deleting the caplike domain of BPO-A2 and further fine-tuning the newly formed substrate binding site. The lipase activity was successfully transplanted on BL1, while the halogenation activity was totally lost. BL1 also showed higher hydrolytic activities toward long chain *p*-nitrophenyl esters, such as *p*-nitrophenyl caprylate (3.7-fold) and *p*-nitrophenyl palmitate (7.0-fold), while its activity toward a short chain ester (*p*-nitrophenyl acetate) decreased dramatically, to only 1.2% of that of BPO-A2. After two rounds of directed evolution and site-directed mutagenesis on selected residues, several mutants with both improved hydrolytic activities and substrate preferences toward long chain substrates were obtained. The highest hydrolytic activity toward *p*-nitrophenyl palmitate of the best mutant BL1-2-E8-plusI was improved by 40-fold compared with that of BL1. These results demonstrate the possibility of manipulating the caplike domain of α/β-hydrolase fold enzymes and provide further understanding of the structure−function relationship of the α/β-hydrolase fold enzymes. The design strategy used in this study could serve as a useful approach for constructing variants with targeted catalytic properties using the α/β-hydrolase fold.

Creating tailor-made enzymes by de novo design has always been a dream of protein engineers. However, because of the limited understanding of the sequence−structure−function relationship of proteins, enzyme design through rational approaches or directed evolution using existing scaffolds of natural enzymes is more practical (*1*−*5*). In particular, in recent years, successful alterations of the catalytic characteristics of one enzyme (scaffold protein) to that of another with a similar scaffold (template protein) have been reported for members of the αβ/βα-metallohydrolase fold (*6*), α/β-hydrolase fold (*7*, *8*), and $(\beta\alpha)_8$-barrel fold (*9*) families and several others (*10*). The strategy involved manipulation of the scaffold protein guided by sequence or structure comparison between the scaffold and the template proteins. For many of these alterations, only a few key residues of the scaffold protein were mutated (*3*, *10*), while limited other cases involved insertion, deletion, or substitution of functional secondary structure elements of the scaffold protein to mimic the structure of the template protein (*6*−*8*).

Among the protein folds with successful alterations between members, the α/β-hydrolase fold represents a functionally versatile protein architecture and a number of enzymes in this fold have important applications in biocatalysis. This fold can tolerate large insertions that form lids and caps that play important roles in defining substrate-binding pockets and regulating the accessibility of active sites. Therefore, it is useful to improve our understanding of the plasticity of this protein fold for enzyme design (*11*, *12*).

In this study, we explore the possibility of converting a heme-free haloperoxidase to a lipase by manipulating the secondary structure elements and residues in and around the substrate binding site. Both enzymes belong to the α/β-hydrolase fold family. The scaffold protein bromoperoxidase A2 (BPO-A2)[1] is a thermostable heme-free haloperoxidase from *Streptomyces aureofaciens* with a funnel-shaped substrate binding pocket (*13*) and a promiscuous esterase activity toward short chain fatty acid esters (*14*), such as *p*-nitrophenyl acetate (*p*NPA). Its scaffold contains a central eight-stranded β-sheet flanked by two helices on one side and three helices on the other side. Between strands β6 and β7, a large caplike insertion is formed by five additional helices, labeled D_1'−D_4' and D (Figures 1A and 2) (*13*). The template enzyme for structure comparison is lipase A from

[†]This work was supported by the National Natural Science Foundation of China (20576062) and the National Basic Research Program of China (2003CB716002).

*To whom correspondence should be addressed. Z.L.: phone, +86-10-62794403; fax, +86-10-62770304; e-mail, zhanglinlin@mail.tsinghua.edu.cn. J.P.: phone, +49-711-685-63191; fax, +49-711-685-63196; e-mail, Juergen.Pleiss@itb.uni-stuttgart.de.

[1]Abbreviations: BPO-A2, bromoperoxidase A2 from *S. aureofaciens*; LipA, lipase A from *B. subtilis*; *p*NPA, *p*-nitrophenyl acetate; *p*NPC, *p*-nitrophenyl caprylate; *p*NPP, *p*-nitrophenyl palmitate; MCD, 2-chloro-5,5-dimethyl-1,3-cyclohexanedione; LB, Luria-Bertani; Kan, kanamycin; IPTG, isopropyl β-thiogalactopyranoside; $SA_{pNPC/pNPA}$, ratio of the specific activities toward *p*NPC and *p*NPA; $SA_{pNPP/pNPA}$, ratio of the specific activities toward *p*NPP and *p*NPA; MD, molecular dynamics; rmsd, root-mean-square deviations; rmsf, root-mean-square fluctuations.

 Published on Web 11/03/2009

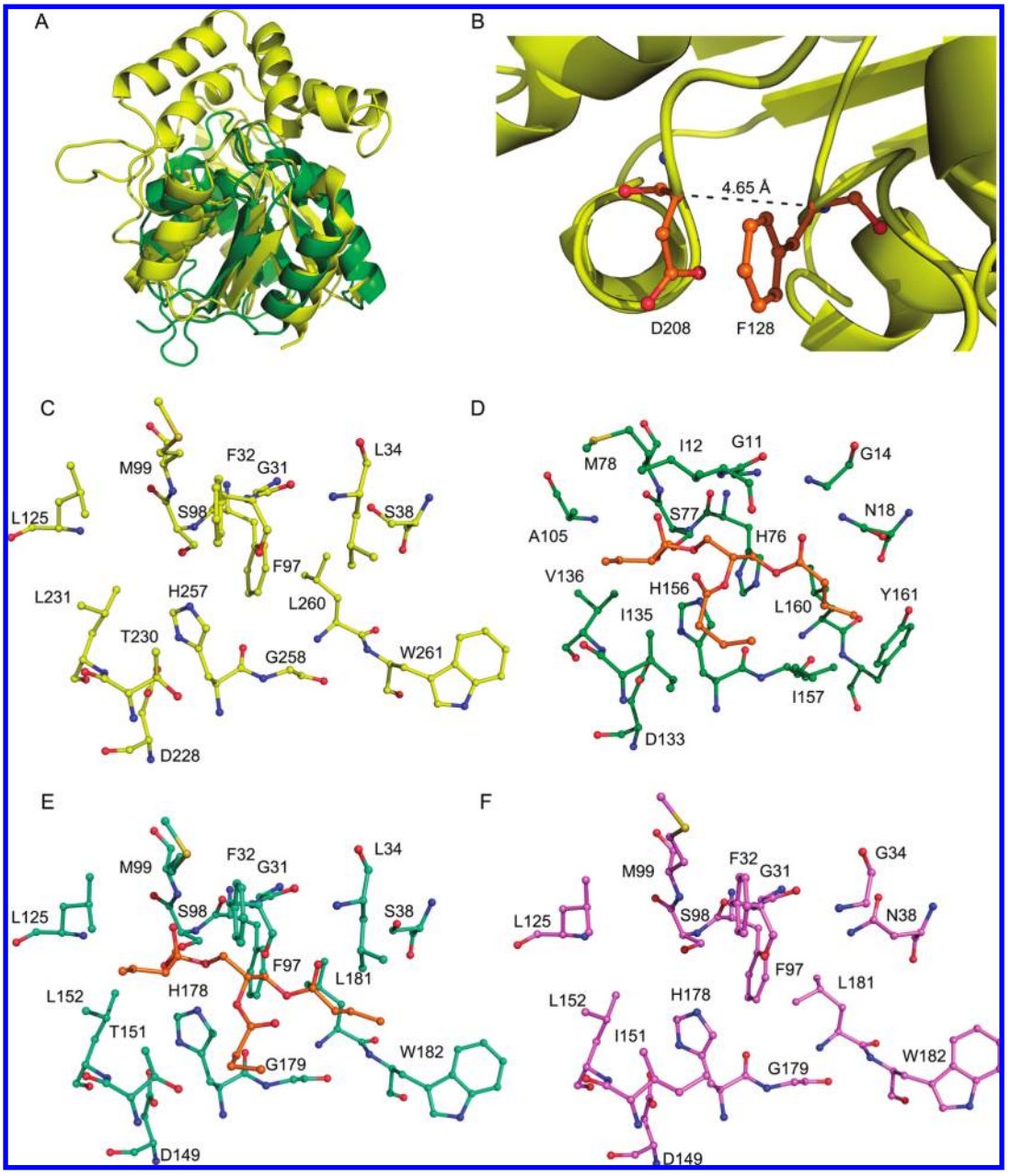

FIGURE 1: (A) Superimposition of the structures of BPO-A2 (yellow) and LipA (green) in a cartoon representation rendered by PyMOL. (B) Distance between the respective Cα atoms of residues F128 and D208 of BPO-A2. (C) Substrate binding site residues of BPO-A2. Oxygen and nitrogen atoms are colored red and deep blue, respectively. The residues located in the caplike domain have been omitted for the sake of clarity. (D) Substrate binding site residues of LipA docked with tributyrin (orange). (E) Substrate binding site residues of BPO-A2-del docked with tributyrin. (F) Substrate binding site residues of BL1. For the sake of clarity, the docking of tributyrin is not shown.

Bacillus subtilis (LipA), which is one of the smallest α/β-hydrolase fold enzymes without a lid. The active site of LipA is solvent-exposed, and its substrate binding site looks like a shallow cleft (*15*). The two enzymes have the same catalytic residues (catalytic triads), similar structures (2.1 Å rmsd), but a very low level of sequence identity (~18%). By removing the caplike domain of BPO-A2 and fine-tuning the residues in the substrate binding site, followed by random and site-directed mutagenesis, we obtained several mutants with improved activity toward long chain fatty acid esters. The plasticity of the BPO-A2 scaffold and the effect of mutations were discussed.

MATERIALS AND METHODS

Reagents. Substrates *p*-nitrophenyl acetate (*p*NPA), *p*-nitrophenyl caprylate (*p*NPC), *p*-nitrophenyl palmitate (*p*NPP), and 2-chloro-5,5-dimethyl-1,3-cyclohexanedione [monochlorodimedon (MCD)] were from Sigma-Aldrich (St. Louis, MO). Isopropyl β-thiogalactopyranoside (IPTG) was from Amresco (Solon, OH). Sodium deoxycholate was from Inalco (San Luis Obispo, CA). Olive oil was from a local supermarket. All the other reagents were of analytical grade. Kits for plasmid extraction and DNA purification were purchased either from QIAGEN (Hilden, Germany) or from TIANGEN (Beijing, China). *Taq* polymerase and DNaseI were obtained from Takara (Dalian, China). Restriction enzymes and T4 DNA ligase were from New England Biolabs (Ipswich, MA). Lysozyme was from Dingguo (Beijing, China). Standard DNA and proteins were purchased from TIANGEN. Oligonucleotides were synthesized by Takara.

Cloning and Expression. The whole-length genes of BPO-A2 and the designed variant BL1 were synthesized and inserted

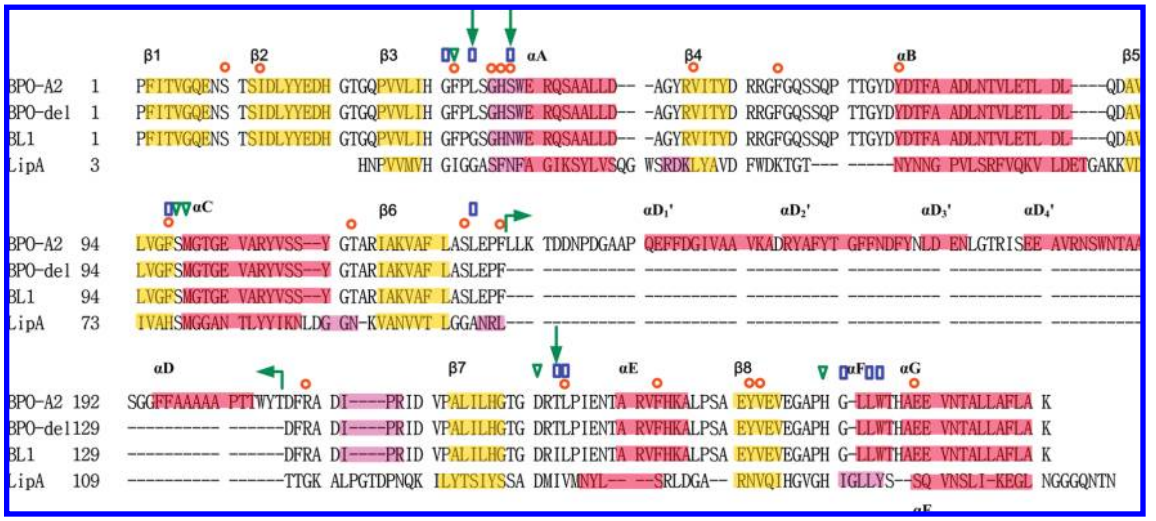

FIGURE 2: Structure-based sequence alignment of BPO-A2, BPO-A2-del, BL1, and LipA assigned with secondary structures (α-helix with a red background, 3_{10}-helix with a purple background, and β-strand with a yellow background). The manipulated secondary structure elements and the three mutated residues are indicated by green arrows. The catalytic triads and oxyanion holes (green hollow triangles), other proposed substrate binding site residues (blue hollow rectangles), and mutated residues obtained in the directed evolutions (orange hollow circles) are also indicated.

into plasmid pET30a using *Nde*I and *Hin*dIII restriction sites by GENEART (Regensburg, Germany). Both genes were linked with a His_6 tag at the C-terminus for purification. *Escherichia coli* strain BL21(DE3) was utilized as a host for cloning and expression. Recombinant strains were routinely cultivated at 37 °C in Luria-Bertani (LB) broth supplemented with kanamycin (Kan, 50 μg/mL). When the optical density at 600 nm (OD_{600}) reached 0.4−0.6, 0.2 mM IPTG were added to the cultures. After induction for 6 h at 30 °C, the cells were harvested by centrifugation.

Comparative Modeling. The three-dimensional (3D) coordinates of BPO-A2-del were constructed by MODELLER version 9.1 (*16*) using the BPO-A2 structure [Protein Data Bank (PDB) entry 1bro (*13*)] as the template. Ten models were created, and the one with the lowest value of MODELLER objective function was chosen as the final model. The quality of the model was then examined by PROCHECK (*17*). The 3D coordinates of BL1 and its mutants were built by using the mutagenesis function in PyMOL version 0.99 (*18*).

Substrate Docking. To identify the possible residues comprising the substrate binding sites of BPO-A2-del and LipA, FlexX2.1 (BioSolveIT, Sankt Augustin, Germany) was utilized to perform covalent docking with tributyrin as the substrate. Atoms O^{γ} and C^{β} of the catalytic residue serine were mapped to the corresponding oxygen and carbon atoms of tributyrin, mimicking the transition state when the hydrolysis reaction takes place. The residues, 15 Å from O^{γ} of the catalytic residue serines, were defined as the pockets of the proteins. The atom types of the conserved histidines of the catalytic triads were assigned to HIS+.

MD Simulation. Molecular dynamics (MD) simulations of BPO-A2 and BL1 were performed on the BioCORTEX cluster at University Stuttgart using the Amber10 program package (*19*). The FF99SB force field and a TI3P water molecule box, with a shortest distance of 10 Å between the wall of the box and the atoms in the solute, were applied. Na^+ was used to neutralize the unit. A total of 5000 steps of energy minimization was performed, with the first 2000 steps being the steepest descent and the rest being the conjugate gradient. To heat and equilibrate the protein and solvent systems, three stages of MD simulation were performed at a constant temperature of 310 K and a constant pressure of 1 bar, with the following constraint forces at each stage: (1) for all atoms, 10.0 kcal mol^{-1} $Å^{-2}$; (2) for the backbone α-carbon, nitrogen, and oxygen atoms only, 5.0 kcal mol^{-1} $Å^{-2}$; (3) for the backbone α-carbon, nitrogen, and oxygen atoms only, 1.0 kcal mol^{-1} $Å^{-2}$. The nonbonded cutoff was set to 8 Å. The length of each step in every stage was 0.001 ps, and the total length of each stage was 100, 200, and 200 ps, respectively. The SHAKE algorithm was applied to fix all bond lengths involving a hydrogen atom. Then a 10 ns MD simulation at 310 K without any constraint for each protein was conducted with the same parameters as shown above. For each protein, the simulation was run three times with different random number generator seeds (IG) for different initial velocity distributions. The root-mean-square deviations (rmsd) of all backbone atoms of the simulated conformations relative to the initial conformation, as well as the root-mean-square fluctuations (rmsf) of residues (the average deviation over time between the conformations of a particular residue at each step, 0.001 ps in this study, and its time-averaged conformation) within the last 4 ns of each simulation, were calculated.

Enzyme Purification. Enzyme-producing cells were harvested, centrifuged, resuspended in buffer A [20 mM sodium phosphate buffer (pH 7.4) containing 500 mM NaCl and 30 mM imidazole], and sonicated. The supernatant was filtered through a 0.2 μm Acrodisc Syringe Filter (Pall, Ann Arbor, MI) and loaded on a Ni^{2+}-charged 5 mL HiTrap Chelating HP column (Amersham Biosciences, Sunnyvale, CA) pre-equilibrated with cold buffer A on an ÄKTA Explorer station (Amersham Pharmacia Biotech, Uppsala, Sweden). The proteins were eluted with a mixture of cold buffer A and buffer B [20 mM sodium phosphate buffer (pH 7.4) containing 500 mM NaCl and 500 mM imidazole] (volume ratio 2:3). The fractions containing target enzymes were changed into lysis buffer [50 mM Tris-HCl buffer (pH 7.2) containing 50 mM NaCl and 5% (v/v) glycerol] with a 10K Amicon Ultra-4 centrifugal filter (Millipore, Billerica, MA). The purities of the enzymes were more than 95% as estimated by sodium dodecyl sulfate−polyacrylamide gel electrophoresis (SDS−PAGE) (12% acrylamide resolving gel and 5% acrylamide stacking gel). The concentrations of the purified enzymes

were determined by measuring the absorbances at 280 nm using extinction coefficients (Table S1 of the Supporting Information) calculated by the ProtParam tool of ExPASy (*20*) according to the composition of amino acids (*21*).

Enzyme Assay. The hydrolytic activity against olive oil was qualitatively tested by dropping 12 nmol of enzymes onto circular areas (~0.7 mm in diameter) of an olive oil/Rhodamine B agar plate (LB/agar plates containing 0.01 mg/mL Rhodamine B and 0.03 mL/mL olive oil) (*22*). The plate was incubated at 37 °C for 10 h and then observed under UV radiation.

The hydrolytic activities were determined by measuring the amount of *p*-nitrophenolate released during enzymatic hydrolysis of different *p*-nitrophenyl esters (*23*), which were monitored at 400 nm with a SpectroMAX M2^e multidetection microplate reader (Molecular Devices, Sunnyvale, CA) at 37 °C. The reaction buffer contained 50 mM sodium phosphate buffer (pH 8.0), 2.07 mg/mL sodium deoxycholate, and 1 mg/mL arabic gum. Substrate (*p*NPA, *p*NPC, or *p*NPP) was first dissolved in 2-propanol and then mixed with reaction buffer by vortexing. Unless otherwise indicated, the final concentrations of ester substrates were all 1.43 mM. The reaction was started by mixing 190 μL of reaction buffer containing substrate with 10 μL of enzyme solution. One unit of hydrolytic activity was defined as the amount of enzyme releasing 1 μmol of *p*-nitrophenolate from *p*-nitrophenyl esters per minute. Measurements were corrected for background hydrolysis in the absence of enzyme. The extinction coefficient of *p*-nitorphenol is 15030 M^{-1} cm^{-1} at 400 nm measured under the standard assay conditions.

The halogenation activity was determined by following the bromination of MCD (*24*). The decrease in absorbance at 290 nm was monitored with a SpectroMAX M2^e multidetection microplate reader at 37 °C. The reaction mixture contained 50 μM MCD, 100 mM NaBr, and 50 mM H_2O_2 in 100 mM sodium acetate buffer (pH 4.1 and 6.0). The reaction was started by addition of 10 μL of an enzyme solution to 190 μL of reaction solution. One unit of halogenation activity was defined as the amount of enzyme catalyzing the consumption of 1 μmol of MCD per minute. The extinction coefficient of MCD is 19900 M^{-1} cm^{-1} (*24*).

Although the thermostability of BL1 decreased greatly, the activities of BL1 and its mutants decreased only 5% after incubation at 40 °C for 30 min. Both the hydrolytic activity and halogenation activity assays were performed at 37 °C for 10 min, and only the initial 5 min was taken for calculation of the specific activities, during which the enzymes should remain intact.

Construction and Screening of a Random Mutant Library. Random mutations were introduced into template genes by error-prone PCR (*25*) with 0.25 mM Mn^{2+} and each primer at 0.3 μM (BL-FOR, 5′-ctt taa gaa gga gat ata cat atg-3′; dI-REV, 5′-gag tgc ggc cgc aag ctt tta-3′). An average of two to three point mutations and one to two amino acid changes per gene were generated, corresponding to a theoretical library size of 2.8×10^6 to 2.2×10^9 (*26*). The amplified DNA fragments were digested with *Nde*I and *Hin*dIII restriction enzymes and ligated by T4 DNA ligase into the similarly digested pET30a vector backbone. The ligation products were transformed into *E. coli* BL21(DE3), and the transformants were plated onto LB agar plates containing 50 μg/mL Kan and incubated at 37 °C overnight. For the two rounds of evolution, 35000 and 50000 single colonies were obtained, respectively, of which ~10% were actually screened in each round. Single colonies were randomly picked with toothpicks and inoculated into 200 μL of LB/Kan medium in 96-well microtiter plates and simultaneously onto LB/Kan agar plates as replications. The parent strains and BL21-(DE3) with only pET30a were used as positive and negative controls, respectively. The cultures were incubated for 15 h at 37 °C. Twenty microliters of overnight culture in each well was inoculated into 1 mL of LB/Kan medium in 96-deepwell plates. These deepwell plates were incubated at 37 °C for 1.5 h, and the expression of enzymes was induced with IPTG at a final concentration of 0.2 mM at 30 °C. Cells were harvested after 6 h, and the medium in each well was removed by centrifugation. The cells were resuspended with 100 μL of lysis buffer containing 0.5 mg/mL lysozyme and 4 units/mL DNaseI, frozen with liquid nitrogen for 2 min, and then thawed at 37 °C for 1 h. After recentrifugation, 20 μL of supernatant from each well was mixed with 180 μL of reaction buffer containing *p*NPC as the substrate for the hydrolytic activity assay. The reaction temperature was set at 30 °C because the standard deviation would be smaller than 37 °C according to previous tests (data not shown). The activity was normalized against the OD_{600} value for each well. The improved mutants were confirmed by growing the cells in tubes and assayed using identical procedures at 37 °C.

Thermostability. Purified enzymes were incubated in triplicate for 30 min at different temperatures in a PCR thermocycler for precise temperature control. The residual activities were measured with *p*NPA as the substrate under the standard conditions described above to yield the thermostability profiles. T_h values (temperature at which half of the protein was denatured) were calculated from the temperature−residual activity curves via linear interpolation.

Site-Directed Mutagenesis. Overlapping PCR was used to introduce specific single mutations/insertion or create saturation mutagenesis of a single site. An isoleucine was inserted after H178 in BL1, BL1-2-E8, and BL1-2-E8(F97Y) via overlapping PCR by using two pairs of primers: BL-FOR (see above) and plusI-Rev (5′-ggt cca cag cag acc aat atg cgg cgc acc ttc-3′) and plusI-For (5′-gaa ggt gcg ccg cat att ggt ctg ctg tgg acc-3′) and PB-R (5′-ggg gtt atg cta gtt att gct-3′). The PCR prodcuts were digested with *Nde*I and *Hin*dIII, cloned into similarly digested pET30a, and transformed into *E. coli* BL21(DE3).

Libraries of saturation mutagenesis at position 97 for BL1-plusI and BL1-2-E8 were constructed via overlapping PCR by using these two pairs of primers: BL-FOR and F97mut-Rev (5′-gcc ggt gcc cat gct nnn gcc aac cag cac cgc atc ctg cag a-3′) and F97mut-For (5′-gcg gtg ctg gtt ggc nnn agc atg ggc acc ggc gaa gt-3′) and PB-R.

RESULTS

Structure Comparison. A structure-based sequence alignment of BPO-A2 and LipA [PDB entries 1bro (*13*) and 1r50 (*27*)] was performed through superimposition of the corresponding catalytic triads, and the backbone atoms of the oxyanion holes (F32 and M99 in BPO-A2 and I12 and M78 in LipA), using Swiss-PdbViewer (*28*), and was visualized in PyMOL. The superimposition results and the structure-based sequence alignment are shown in Figure 2. The catalytic triads of both enzymes superimposed quite well with a rmsd of 0.481 Å, but the shapes of the substrate binding sites were quite different. In BPO-A2, the catalytic triad was composed of S98, D228, and H257 and located at the end of a 10.0−15.0 Å deep funnel-like pocket (*13*). The hydrophobic fatty acid binding pocket is located inside the

enzyme and formed by residues L129, F163, and W205 from the caplike domain on the top and residues F32, M99, L125, T230, and L231 at the bottom. Its length is less than 8 Å, which restricts the substrate specificity of BPO-A2 to short chain esters. The size of the alcohol binding pocket of BPO-A2 is very small, which is underestimated as it is derived from a substrate-free structure (*29*). While in LipA, the corresponding catalytic residues were S77, D133, and H156 and located at the bottom of the substrate binding cleft. The fatty acid binding groove is lined by residues I12, M78, A105, L108, I135, and L140, and the alcohol binding groove is formed by residues 12−18 and residues 157−161 (*15*, *27*). The major structural difference between the two enzymes is the caplike domain of BPO-A2, an insert of 79 amino acids between strands β6 and β7, which is lacking in LipA.

The engineering of BPO-A2 for lipase activity was performed in three steps: (1) removal of the cap region of BPO-A2 and fine-tuning of the substrate binding site by site-directed mutagenesis, (2) improvement of the catalytic activity by two rounds of directed evolution, and (3) saturation mutagenesis and combination of mutations.

Step 1: Removal of the Cap Region and Fine-Tuning of the Substrate Binding Site. In the first step, the cap domain [residues 129−207 (Figures 1A and 2)] was removed. Residues F128 and D208 in two spatially adjacent loop regions were connected directly, as the distance between the respective Cα atoms was only 4.65 Å, which was suitable for formation of a new peptide bond between them (Figure 1B). A model of BPO-A2-del was constructed; more than 99% of the residues were in the favorable (Φ, Ψ)-region, while only the nucleophile (S98) had unfavorable main chain torsion angles which is common for nucleophiles in α/β-hydrolase fold enzymes (*30*). To identify substrate-interacting residues, the conformation of the side chain of the nucleophile serine was changed to its active state by rotating the side chain (*31*) and a tributyrin substrate molecule was docked to the active site with the *sn*-1 moiety binding to the acid binding pocket and the *sn*-2,3-diglyceride to the alcohol binding pocket. Fourteen residues were inferred to constitute the substrate binding sites in BPO-A2-del and LipA (Figure 1D,E). Residue S98 in BPO-A2 (corresponding to S77 in LipA) and H178 (H156) are part of the catalytic triad. The backbone nitrogen atoms of F32 (I12) and M99 (M78) form the oxyanion hole. Residues G31/G11, L125/A105, L152/V136, L181/L160, and W182/Y161 bind to the substrate and either are identical in both enzymes or have similar physicochemical properties and therefore were not changed in BPO-A2-del. Residue F97 (H76) is located before the nucleophile serine S98 (S77). To avoid a possible deleterious effect on the catalytic triad of BPO-A2-del, F97 in BPO-A2-del was not altered either. For the same reason, residue G179 (I157) located after the catalytic residue histidine H178 (H156) was also not changed, although an insertion of an isoleucine between H178 and G179 gives a better mimic of this substrate binding region of LipA from the point of view of sequence identity (Figure 2). The other significant differences lie in three pairs (L34/G14, S38/N18, and T151/I135) that differed either in side chain size or in hydrophobicity. Thus, three residues were mutated in BPO-A2-del (L34G, S38N, and T151I), and the model structure of the construct BL1 was created.

To investigate the possible effect of the deletion of the cap domain (corresponding to 30% of the total residues in BPO-A2) on the stability of BL1, three 10 ns MD simulations of BL1 and BPO-A2 with different initial velocities and the calculation of the possible number of salt bridges on the surface of proteins were

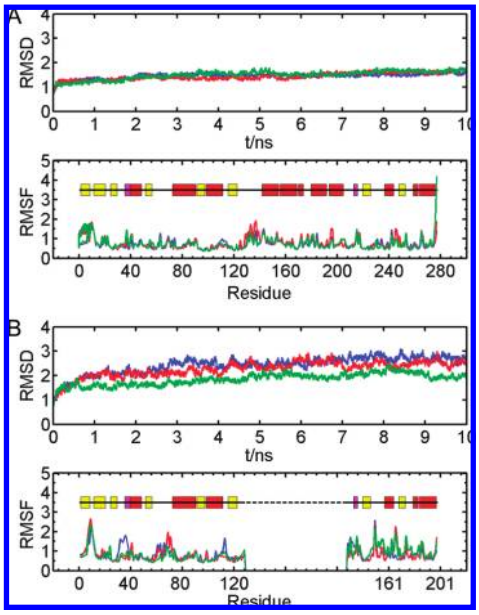

FIGURE 3: (A) rmsd and rmsf plots of 10 ns MD simulations of BPO-A2. (B) rmsd and rmsf plots of 10 ns MD simulations of BL1. For each protein, three simulations with different initial velocities were conducted, and the curves are colored with red, blue, and green. Red, yellow, and purple boxes stand for α-helix, β-strand, and 3_{10}-helix, respectively. The unit is angstroms.

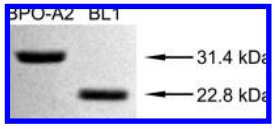

FIGURE 4: SDS−PAGE of purified BPO-A2 and BL1.

conducted. The rmsd plot of the 10 ns MD simulations showed that the conformation of BL1 gradually changed and no significant unfolding occurred (Figure 3B). However, the backbone root-mean-square deviation between the final and initial structure of BL1 was slightly larger than that between the final and initial structures of BPO-A2. The analysis of the root-mean-square fluctuation of the backbone atoms (Figure 3) demonstrated that the flexibility of three loops increased as compared to the corresponding loops in BPO-A2: loop L1 (between strand β1 and β2), L5 (between strand β4 and helix αB), and L12 (between strand β7 and helix αE). In BPO-A2, these three loops interact with the cap domain: loop L5 interacts with loops L1 and L9 (between helix $\alpha D_4'$ and αD); loop L12 interacts with helix $\alpha D_2'$. The deletion of the cap domain in BL1 seems to liberate these loops, increase the flexibility, and thus might reduce the stability of the protein. As calculated by VMD (*32*) (the nitrogen−oxygen distance cutoff was set to 4.5 Å, the upper limit for salt bridges), the numbers of possible salt bridges on the surface of BPO-A2 and BL1 are 19 and 14, respectively. There is no new salt bridge forming on the newly exposed surface.

Expression and Characterization of BL1. The genes of BPO-A2 and BL1 were synthesized and linked with His_6 tags at the C-terminus for purification. SDS−PAGE of purified BL1 showed that it could be expressed under the standard cultivation conditions (Figure 4). The purified BL1 had a tendency to aggregate and precipitate in solution under slightly alkaline conditions (pH 7.2 in lysis buffer and pH 7.4 in a mixture of bufferA and buffer B; also see Materials and Methods), similar to LipA (*33*). The purified BPO-A2 and BL1 were tested for their

lipase activities on olive oil/Rhodamine B agar plates. For BL1, but not for BPO-A2, a very weak fluorescence under UV radiation was observed (Figure 5A), which demonstrated that BL1 exhibited a weak lipase activity toward triglycerides. However, this activity was too low to be measured by titration (*34*) (data not shown).

The specific hydrolytic activities of BL1 and BPO-A2 were measured against *p*-nitrophenyl esters containing different numbers of carbon atoms in the fatty acid chains under standard conditions: *p*NPA (C2), *p*NPC (C8), and *p*NPP (C16).

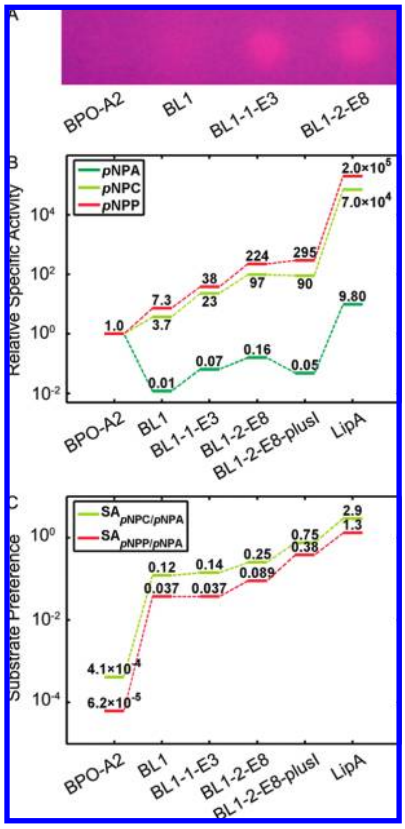

FIGURE 5: (A) Lipase activity detected on an olive oil/Rhodamine B plate. (B) Relative specific activities and (C) substrate preferences of BPO-A2, BL1, and the best mutants in each round of directed evolution and site-directed mutagenesis toward *p*NPA, *p*NPC, and *p*NPP.

The results showed that BL1 had higher activities toward *p*NPC (3.7-fold) and *p*NPP (7.3-fold) than BPO-A2, but the activity toward *p*NPA decreased greatly, only 1.2% of that for BPO-A2 (Table 1 and Figure 5B). The ratios of the activity toward *p*NPC or *p*NPP to that of *p*NPA (Figure 5C and Table S2 of the Supporting Information) ($SA_{pNPC/pNPA}$ or $SA_{pNPP/pNPA}$, respectively) were calculated to evaluate the substrate preferences of the enzymes. For BPO-A2, these values were 4.1×10^{-4} and 6.2×10^{-5}, respectively, while for BL1, these values were 1.2×10^{-1} and 3.6×10^{-2}, respectively. Therefore, there was an increase of ~300−600-fold in terms of substrate preferences for long chain esters (*p*NPC or *p*NPP) for BL1, compared to BPO-A2.

We wish to mention that while the preferred parameters for comparing the substrate specificities would be the values of k_{cat}/K_M for the tested substrates and enzymes, the measurements of these parameters in this study were hampered by the low activities of the evolved enzymes and the low substrate solubility of *p*NPP (see Table S3 of the Supporting Information). Thus, as an alternative, we used the ratios of specific activities at a fixed concentration for all substrates as indicators for substrate preferences, which are used widely for mapping substrate specificity of lipases or esterases toward *p*-nitrophenyl esters (*35*−*38*) (also see Note 1 of the Supporting Information).

The specific halogenation activities of BPO-A2 and BL1 were first measured at pH 4.5, which was the optimal pH of BPO-A2 (*39*). However, BL1 formed a white precipitation in the pH range from 4.5 to 5.5. Reaction mixtures at pH 4.1 and 6.0 were thus chosen for the halogenation activity assay. BPO-A2 showed an activity of 23 ± 2 units/μmol of enzyme at pH 4.1 and 2.7 ± 0.1 units/μmol of enzyme at pH 6.0. BL1 showed no detectable halogenation activity under both pH conditions (Table 1).

The thermostability of BL1 decreased dramatically compared to that of BPO-A2, which is consistent with the MD simulation results. The T_h value of BPO-A2 is 81.9 °C, while the T_h of BL1 is only 45.1 °C.

Step 2: Directed Evolution of BL1. Directed evolution via error-prone PCR was conducted on BL1 to increase the hydrolytic activity. In the first round, a total of 3518 mutants were screened in 96-well microtiter plates and confirmed in tubes with *p*NPC as the substrate. Eight mutants with increased activities were sequenced (Table S4 of the Supporting Information) and purified. The specific activities of these mutants toward different

Table 1: Specific Activities and Substrate Preferences of Selected Enzymes

	specific activity (units/μmol of enzyme)			
	*p*NPA[a]	*p*NPC[a]	*p*NPP[a]	MCD[b]
BPO-A2	106 ± 02	0.043 ± 0.003	0.0066 ± 0.0004	23 ± 2
LipA	(1.04 ± 0.06) × 10^3	(3.0 ± 0.3) × 10^3	(1.3 ± 0.2) × 10^3	—[c]
BL1	1.31 ± 0.03	0.161 ± 0.004	0.048 ± 0.001	ND[d]
BL1-1-E3	6.89 ± 0.09	0.99 ± 0.06	0.252 ± 0.003	ND[d]
BL1-2-E8	16.7 ± 0.4	4.16 ± 0.08	1.48 ± 0.02	ND[d]
BL1-plusI	0.82 ± 0.02	0.21 ± 0.02	0.094 ± 0.002	—[c]
BL1-plusI(F97Y)	1.01 ± 0.09	0.58 ± 0.02	0.181 ± 0.005	—[c]
BL1-2-E8-plusI	5.1 ± 0.4	3.85 ± 0.09	1.95 ± 0.07	—[c]
BL1-2-E8(F97Y)	26 ± 1	6.3 ± 0.2	1.10 ± 0.04	—[c]
BL1-2-E8-plusI(F97Y)	8.4 ± 0.4	5.7 ± 0.2	1.75 ± 0.02	—[c]
BL1-2-E8-plusI(F97I)	ND[d]	0.61 ± 0.06	1.57 ± 0.04	—[c]

[a]One unit of hydrolytic activity was defined as the amount of enzyme releasing 1 μmol of *p*-nitrophenolate from *p*-nitrophenyl esters per minute. [b]One unit of halogenation activity was defined as the amount of enzyme catalyzing the consumption of 1 μmol of MCD per minute. Measured at pH 4.1. [c]Did not take the measurement. [d]Not detectable.

lengths of fatty acid chain esters were measured under standard conditions, and the substrate preference improvements were calculated (Table 1, Figure 5, and Table S2 of the Supporting Information). Among these mutants, mutant BL1-1-E3 exhibited the highest activities toward *p*NPC and *p*NPP, ~6.1- and 5.3-fold higher than that of BL1, respectively. However, the substrate preference remained unchanged. On the other hand, mutant BL1-1-G9 showed a 2.5-fold increase in substrate preference (measured as the ratio of the specific activities toward *p*NPP and *p*NPA, $SA_{pNPP/pNPA}$), as compared to BL1; however, its activity was much lower than that of BL1-1-E3. Mutant BL1-1-D7 showed a decrease in substrate preference for long chain substrates.

The second round of evolution was conducted with BL1-1-E3 as the template. Seven of 5400 mutants screened were isolated, sequenced (Table S4 of the Supporting Information), and purified. The most active mutant, BL1-2-E8, showed 4.2- and 5.9-fold higher specific activities toward *p*NPC and *p*NPP, respectively (Table 1). Its substrate preferences were also improved to ~1.7-fold ($SA_{pNPC/pNPA}$) and 2.4-fold ($SA_{pNPP/pNPA}$) higher than that of BL1-1-E3 (Figure 5C and Table S2 of the Supporting Information). Other mutants also showed improved substrate preferences; for example, the less active mutant BL1-2-D10 showed the greatest improvement, 2.6-fold for $SA_{pNPC/pNPA}$ and 3.2-fold for $SA_{pNPP/pNPA}$ (Table S2 of the Supporting Information). The substrate preferences of these improved mutants were only 1 order of magnitude lower than that of LipA (Figure 5C and Table S2 of the Supporting Information).

The fluorescence produced by BL1-1-E3 and BL1-2-E8 on Rhodamine B/olive oil plates under UV radiation was much stronger than that of BL1 (Figure 5A), which means the activities toward triglycerides are also improved, but the exact activities were still too low to be determined by the standard titration assay.

For the halogenation activity measurements, mutants BL1-1-E3 and BL1-2-E8 again formed white precipitation at pH 4.5−5.5, and at pH 4.1 and 6.0, no halogenation activity was detected (Table 1).

Sequence analysis of the mutants showed that 50% of the mutations occur at the substrate binding sites or have direct contact with the substrate binding site residues. For several positions (H37, N38, F61, Y73, L152, and F161), mutations occurred more than once (Table S4 of the Supporting Information).

Step 3: Insertion of an Isoleucine after H178 Coupled with Saturated Mutagenesis at F97. In the first round of evolution, mutant BL1-1-D7 with mutation F97Y showed a 1.9-fold activity toward *p*NPC compared to BL1. This result suggested that the mutations adjacent to the catalytic triad would also be beneficial to the catalytic activity. To judge the effect of this mutation on BL1-2-E8, saturation mutagenesis at this position in BL1-2-E8 was conducted and screened in 96-well microtiter plates with *p*NPC as the substrate. Four improved BL1-2-E8 mutants were isolated from a library of ~150. Strikingly, sequencing revealed that all these mutants have the same F97Y mutation. The specific activities of the purified enzyme were slightly higher toward *p*NPC (1.5-fold) as well as *p*NPA (1.6-fold), but lower toward *p*NPP (74%). As a result, the $SA_{pNPC/pNPA}$ value remained unchanged, and the $SA_{pNPP/pNPA}$ value was lowered to 0.042 (Table S2 of the Supporting Information).

We were also prompted to take a second look at G179. G179 is the C-terminal neighbor of H178 and is located before short α-helix αF of BL1 which contains two substrate binding residues. Its corresponding residue in LipA, I156, is part of a short 3_{10}-helix (Figure 2). To better mimic LipA in this region for substrate binding, an isoleucine was inserted between H178 and G179 in BL1 and its variant BL1-2-E8, yielding BL1-plusI and BL1-2-E8-plusI, respectively. Both of the purified enzymes were found to exhibit higher activities toward *p*NPP (2.0- and 1.3-fold) and lower activities toward *p*NPA (63 and 31%), resulting in a greater substrate preference toward long chain substrates than their parent enzymes (Table 1 and Table S2 of the Supporting Information). The values of $SA_{pNPC/pNPA}$ and $SA_{pNPP/pNPA}$ of BL1-2-E8-plusI were increased to 0.75 and 0.38, respectively, and were ~30% of those of LipA (Figure 5C). However, the insertion of an isoleucine reduced the expression level of BL1-2-E8-plusI by more than 50% (data not shown).

Saturation mutagenesis at position 97 was also conducted in BL1-plusI, and two improved BL1-plusI mutants were isolated. Once again, sequencing showed that these two mutants carried the same F97Y mutation. Purified BL1-plusI(F97Y) exhibited higher specific activities toward *p*NPC (2.8-fold), *p*NPP (1.9-fold), and *p*NPA (1.2-fold) as compared to BL1-plusI. As a result, $SA_{pNPC/pNPA}$ and $SA_{pNPP/pNPA}$ were increased to 0.57 and 0.18, respectively (Table 1 and Table S2 of the Supporting Information). Mutant BL1-2-E8-plusI(F97Y) was further constructed by introduction of the isoleucine between position 178 and 179 in BL1-2-E8(F97Y) through overlapping PCR. The purified BL1-2-E8-plusI(F97Y) showed higher activities against *p*NPC (1.4-fold) and *p*NPP (1.2-fold), and lower activity against *p*NPA (50%) (Table 1), resulting in higher $SA_{pNPC/pNPA}$ (2.8-fold) and $SA_{pNPP/pNPA}$ (2.4-fold) versus those of BL1-2-E8 (Table S2 of the Supporting Information).

It was very interesting that an unexpected mutant BL1-2-E8-plusI(F97I) carrying the F97I mutation was found. This mutant totally lost the activity toward *p*NPA and exhibited 9.4-fold lower activity toward *p*NPC than the parent, while maintaining the activity toward *p*NPP (Table 1). The substrate preference of this mutant toward *p*NPP and *p*NPC was inverted, and $SA_{pNPP/pNPC}$ was increased from 0.51 for BL1-2-E8-plusI to 2.6, much higher than that of LipA (0.43) (Table S2 of the Supporting Information). However, the specific activity was still 820-fold lower than that of LipA, and this mutant exhibited a very low solubility (data not shown).

DISCUSSION

By combining rational design and directed evolution, we redesigned BPO-A2 into a LipA-like enzyme. Lipase activity was successfully introduced as demonstrated by the shift of substrate preferences toward long chain esters (*p*NPC and *p*NPP) and by the olive oil/Rhodamine B plate test, accompanied by the total loss of its halogenation activity. In fact, the substrate preferences for *p*NPP and *p*NPC as compared to *p*NPA for the best mutant BL1-2-E8-plusI reach ~30% of those for LipA. While the hydrolytic activity of the best mutant BL1-2-E8-plusI toward *p*NPP is still 660-fold lower than that of LipA, which is comparable to other similar studies where manipulation of large segments of a template protein is involved (*6*, *8*, *40*−*42*). For example, the best mutant obtained by Park and co-workers is ~3 orders of magnitude lower than that of the target human IMP-1 metallo-β-lactamase (IMP-1) (*6*).

The fact that BL1 can be functionally overexpressed suggests that the folding processes of the caplike domain and the core scaffold of BPO-A2 are independent. Similar phenomena have

also been observed when the lid of a lipase was removed (*40*, *43*) or two lipases exchanged their lids with different sizes (*41*, *44*). It also suggests that the lid, cap, or caplike domains of other enzymes in the α/β-hydrolase fold family can also be deleted, inserted, or substituted without disturbing the folding of the core α/β-hydrolase fold domains, which would be very useful for enzyme redesign, especially in constructing a hybrid enzyme for a new activity or substrate profile.

However, the thermostability of BPO-A2 is substantially affected by removal of the caplike domain. Its removal increases the flexibility of BL1, especially the loops that originally have interactions with the caplike domain and cause a reduction in the number of salt bridges from 19 to 14, thereby disrupting electrostatic interactions on the interface (*45*).

Because of the limitations of the rational approach, in many cases for a redesigned protein scaffold, a much lower or even undetectable activity has been obtained as compared to the template protein (*6*, *8*, *40*−*42*), and the geometry of an active site transplanted onto a foreign scaffold often needs further optimization. Park and co-workers (*6*) introduced the β-lactamase activity onto the human glyoxalase II scaffold by mimicking the active site of human IMP-1 metallo-β-lactamase (IMP-1) followed by seven rounds of evolution starting from 13 variants with undetectable β-lactamase activity. Röthlisberger and co-workers (*4*, *46*) created enzymes with Kemp elimination activity by matching de novo-designed active sites with existing scaffolds in nature and improved the activity of one design to the level of a benchmark catalytic antibody 34E4 after seven rounds of evolution. In this study, although BL1 shows detectable lipase activity and a 2 order of magnitude of improvement in the substrate preference toward long chain esters over short chain esters, the hydrolytic activity of BL1 is still much lower compared to that of LipA [$\sim 10^4$-fold lower (Table 1)]. After two rounds of directed evolution, the hydrolytic activities toward *p*NPP and *p*NPC of the best mutant BL1-2-E8 were improved by ∼25−30-fold as compared to that of the initially designed enzyme BL1. While the overall activity could be significantly improved by directed evolution, the improvements in the substrate preference ($SA_{pNPC/pNPA}$ and $SA_{pNPP/pNPA}$) were mainly obtained by rational design of BL1 and site-directed mutagenesis of BL1-2-E8-plusI and did not change considerably upon directed evolution.

By analysis of the crystal structures bound with inhibitors of LipA (*27*) and the results of docking tributyrin to LipA and BPO-A2-del, the role of the mutated residues was analyzed. Alcohol moieties and the fatty acid moieties of the esters and triglycerides are bound to the so-called alcohol binding sites and fatty acid binding sites of the substrate binding clefts, respectively (Figure 6). Among the 15 improved BL1 mutants from directed evolution (Table S4 of the Supporting Information), 12 contain mutations within 3.5 Å of the substrate binding site. While the molecular basis of these mutations for the increased specific activity and the shift of substrate preference is not always evident, two conclusions might be drawn.

The mutations near the fatty acid binding site should affect substrate preference. Y73F in mutant BL1-1-G9 is in direct contact with oxyanion hole residue M99 and proposed substrate binding site residue Leu152. Because this position is far from catalytic residue S98, it can be inferred that this mutation will affect the binding of the fatty acid chain of *p*NPC and *p*NPP but not that of *p*NPA, leading to enhanced preferences toward *p*NPC and *p*NPP.

Moreover, it is interesting to note that those at the proposed alcohol binding site and its spatially adjacent neighbors in BL1

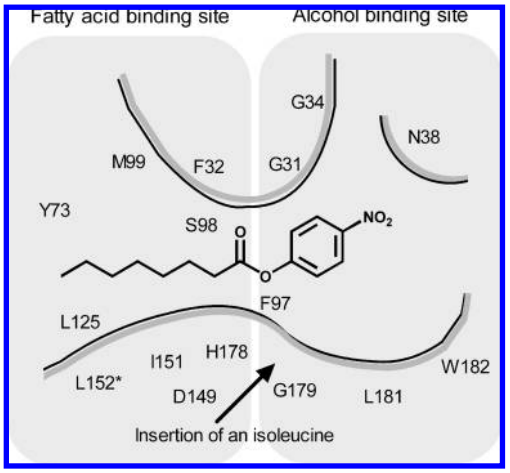

FIGURE 6: Sketch of the substrate binding site of BL1 and a spatially adjacent residue, Y73. The arrow denotes the insertion of an isoleucine between H178 and G179.

variants clearly also affect the preference for the fatty acid chain length of the esters. For instance, mutation N38D in mutant BL1-2-A5 decreases its preferences toward *p*NPP and *p*NPC when compared to those of BL1-1-E3. Insertion of an isoleucine between positions 178 and 179 in BL1-plusI, BL1-2-E8-plusI, and BL1−2-E8-plusI(F97Y) also produces mutants with greater preferences toward *p*NPP and *p*NPC. Most prominently, mutant BL1-2-E8-plusI(F97I) loses its activity toward *p*NPA, a 85% reduction in the activity toward *p*NPC compared to that of BL1-2-E8-plusI, but maintains the same level of activity toward *p*NPP as BL1-2-E8-plusI. As isoluecine is smaller than phenylalanine, a F97I mutation might reduce the affinity for the nitrophenyl group, and thus, the binding of substrate becomes largely dependent on the fatty acid chain moiety, which in turn explains the activity loss for *p*NPA and the reduced activity for *p*NPC with a C8 fatty acid chain.

It is noteworthy that the two residues in LipA (N18 and I157) corresponding to the aforementioned N38 and the inserted isoleucine at position 179 in BL1 variants also play important roles in the enantioselectivity (*7*) and stereoselectivity of LipA (*47*). In particular, I157 in LipA, together with the neighboring catalytic residue H156, forms the so-called His gap motif, which is a determinant of stereoselectivity for many microbial lipases toward triacylglycerols (*47*).

In summary, we have successfully transplanted the lipase activity onto the scaffold of BPO-A2 by a combination of rational design under the guidance of structure comparison with LipA and directed evolution. These results suggest the strategy used in this study is helpful for engineering other α/β-hydrolase fold enzymes.

ACKNOWLEDGMENT

We thank Benjamin Juhl at the Institute of Technical Biochemistry of the University of Stuttgart for his kind technical assistance in enzyme design. We also appreciate Dr. Wei Zhang and Ms. Peichun Wu at Dalian Institute of Chemical Physics for the gift of MCD.

SUPPORTING INFORMATION AVAILABLE

Tables listing extinction coefficients, specific activities, substrate preferences, and kinetic parameters of various enzymes discussed in the main text and saturation curves for BL1-1-E3 and BL1-2-E8. This material is available free of charge via the Internet at http://pubs.acs.org.

REFERENCES

1. Koder, R. L., and Dutton, P. L. (2006) Intelligent design: The *de novo* engineering of proteins with specified functions. *Dalton Trans.,* 3045–3051.
2. Leisola, M., and Turunen, O. (2007) Protein engineering: Opportunities and challenges. *Appl. Microbiol. Biotechnol. 75*, 1225–1232.
3. Toscano, M. D., Woycechowsky, K. J., and Hilvert, D. (2007) Minimalist active-site redesign: Teaching old enzymes new tricks. *Angew. Chem., Int. Ed. 46*, 3212–3236.
4. Röthlisberger, D., Khersonsky, O., Wollacott, A. M., Jiang, L., DeChancie, J., Betker, J., Gallaher, J. L., Althoff, E. A., Zanghellini, A., Dym, O., Albeck, S., Houk, K. N., Tawfik, D. S., and Baker, D. (2008) Kemp elimination catalysts by computational enzyme design. *Nature 453*, 190–195.
5. Jiang, L., Althoff, E. A., Clemente, F. R., Doyle, L., Röthlisberger, D., Zanghellini, A., Gallaher, J. L., Betker, J. L., Tanaka, F., Barbas, C. F., Hilvert, D., Houk, K. N., Stoddard, B. L., and Baker, D. (2008) De novo computational design of retro-aldol enzymes. *Science 319*, 1387–1391.
6. Park, H. S., Nam, S. H., Lee, J. K., Yoon, C. N., Mannervik, B., Benkovic, S. J., and Kim, H. S. (2006) Design and evolution of new catalytic activity with an existing protein scaffold. *Science 311*, 535–538.
7. Boersma, Y. L., Pijning, T., Bosma, M. S., van der Sloot, A. M., Godinho, L. F., Dröge, M. J., Winter, R. T., van Pouderoyen, G., Dijkstra, B. W., and Quax, W. J. (2008) Loop grafting of *Bacillus subtilis* lipase A: Inversion of enantioselectivity. *Chem. Biol. 15*, 782–789.
8. Jochens, H., Stiba, K., Savile, C., Fujii, R., Yu, J. G., Gerassenkov, T., Kazlauskas, R. J., and Bornscheuer, U. T. (2009) Converting an esterase into an epoxide hydrolase. *Angew. Chem., Int. Ed. 48*, 3532–3535.
9. Leopoldseder, S., Claren, J., Jürgens, C., and Sterner, R. (2004) Interconverting the catalytic activities of $(\beta\alpha)_8$-barrel enzymes from different metabolic pathways: Sequence requirements and molecular analysis. *J. Mol. Biol. 337*, 871–879.
10. Berglund, P., and Park, S. (2005) Strategies for altering enzyme reaction specificity for applied biocatalysis. *Curr. Org. Chem. 9*, 325–336.
11. Qian, Z., Fields, C. J., Yu, Y., and Lutz, S. (2007) Recent progress in engineering α/β hydrolase-fold family members. *Biotechnol. J. 2*, 192–200.
12. Heikinheimo, P., Goldman, A., Jeffries, C., and Ollis, D. L. (1999) Of barn owls and bankers: A lush variety of α/β hydrolases. *Structure 7*, R141–R146.
13. Hecht, H. J., Sobek, H., Haag, T., Pfeifer, O., and van Pée, K. H. (1994) The metal-ion-free oxidoreductase from *Streptomyces aureofaciens* has an α/β hydrolase fold. *Nat. Struct. Biol. 1*, 532–537.
14. Kirk, O., and Conrad, L. S. (1999) Metal-free haloperoxidases: Fact or artifact? *Angew. Chem., Int. Ed. 38*, 977–979.
15. van Pouderoyen, G., Eggert, T., Jaeger, K. E., and Dijkstra, B. W. (2001) The crystal structure of *Bacillus subtilis* lipase: A minimal α/β hydrolase fold enzyme. *J. Mol. Biol. 309*, 215–226.
16. Sali, A., and Blundell, T. L. (1993) Comparative protein modelling by satisfaction of spatial restraints. *J. Mol. Biol. 234*, 779–815.
17. Laskowski, R. A., MacArthur, M. W., Moss, D. S., and Thornton, J. M. (1993) PROCHECK: A program to check the stereochemical quality of protein structures. *J. Appl. Crystallogr. 26*, 283–291.
18. DeLano, W. L. (2002) The PyMOL Molecular Graphics System, DeLano Scientific, Palo Alto, CA.
19. Case, D. A., Darden, T. A., Cheatham, T. E., III, Simmerling, C. L., Wang, J., Duke, R. E., Luo, R., Crowley, M., Walker, R. C., Zhang, W., Merz, K. M., Wang, B., Hayik, S., Roitberg, A., Seabra, G., Kolossváry, I., Wong, K. F., Paesani, F., Vanicek, J., Wu, X., Brozell, S. R., Steinbrecher, T., Gohlke, H., Yang, L., Tan, C., Mongan, J., Hornak, V., Cui, G., Mathews, D. H., Seetin, M. G., Sagui, C., Babin, V., and Kollman, P. A. (2008) AMBER 10 , University of California, San Francisco.
20. Gasteiger, E., Gattiker, A., Hoogland, C., Ivanyi, I., Appel, R. D., and Bairoch, A. (2003) ExPASy: The proteomics server for in-depth protein knowledge and analysis. *Nucleic Acids Res. 31*, 3784–3788.
21. Gill, S. C., and von Hippel, P. H. (1989) Calculation of protein extinction coefficients from amino acid sequence data. *Anal. Biochem. 182*, 319–326.
22. Kouker, G., and Jaeger, K. E. (1987) Specific and sensitive plate assay for bacterial lipases. *Appl. Environ. Microbiol. 53*, 211–213.
23. Winkler, U. K., and Stuckmann, M. (1979) Glycogen, hyaluronate, and some other polysaccharides greatly enhance the formation of exolipase by *Serratia marcescens*. *J. Bacteriol. 138*, 663–670.
24. Krenn, B. E., Plat, H., and Wever, R. (1988) Purification and some characteristics of a non-haem bromoperoxidase from *Streptomyces aureofaciens*. *Biochim. Biophys. Acta 952*, 255–260.
25. Joo, H., Lin, Z. L., and Arnold, F. H. (1999) Laboratory evolution of peroxide-mediated cytochrome P450 hydroxylation. *Nature 399*, 670–673.
26. Wedge, D. C., Rowe, W., Kell, D. B., and Knowles, J. (2009) *In silico* modelling of directed evolution: Implications for experimental design and stepwise evolution. *J. Theor. Biol. 257*, 131–141.
27. Dröge, M. J., Boersma, Y. L., van Pouderoyen, G., Vrenken, T. E., Rüggeberg, C. J., Reetz, M. T., Dijkstra, B. W., and Quax, W. J. (2006) Directed evolution of *Bacillus subtilis* lipase A by use of enantiomeric phosphonate inhibitors: Crystal structures and phage display selection. *ChemBioChem 7*, 149–157.
28. Guex, N., and Peitsch, M. C. (1997) SWISS-MODEL and the Swiss-PdbViewer: An environment for comparative protein modeling. *Electrophoresis 18*, 2714–2723.
29. Pleiss, J., Fischer, M., and Schmid, R. D. (1998) Anatomy of lipase binding sites: The scissile fatty acid binding site. *Chem. Phys. Lipids 93*, 67–80.
30. Holmquist, M. (2000) α/β-Hydrolase fold enzymes: Structures, functions and mechanisms. *Curr. Protein Pept. Sci. 1*, 209–235.
31. Kawasaki, K., Kondo, H., Suzuki, M., Ohgiya, S., and Tsuda, S. (2002) Alternate conformations observed in catalytic serine of *Bacillus subtilis* lipase determined at 1.3 Å resolution. *Acta Crystallogr. D 58*, 1168–1174.
32. Humphrey, W., Dalke, A., and Schulten, K. (1996) VMD: Visual molecular dynamics. *J. Mol. Graphics 14*, 33–38.
33. Lesuisse, E., Schanck, K., and Colson, C. (1993) Purification and preliminary characterization of the extracellular lipase of *Bacillus subtilis* 168, an extremely basic pH-tolerant enzyme. *Eur. J. Biochem. 216*, 155–160.
34. Beisson, F., Tiss, A., Rivière, C., and Verger, R. (2000) Methods for lipase detection and assay: A critical review. *Eur. J. Lipid Sci. Technol. 102*, 133–153.
35. Reyes-Duarte, D., Polaina, J., López-Cortés, N., Alcalde, M., Plou, F. J., Elborough, K., Ballesteros, A., Timmis, K. N., Golyshin, P. N., and Ferrer, M. (2005) Conversion of a carboxylesterase into a triacylglycerol lipase by a random mutation. *Angew. Chem., Int. Ed. 44*, 7553–7557.
36. Kim, S. B., Lee, W., and Ryu, Y. W. (2008) Cloning and characterization of thermostable esterase from *Archaeoglobus fulgidus*. *J. Microbiol. 46*, 100–107.
37. Mateos, J. C., Ruiz, K., Rodriguez, J. A., Cordova, J., and Baratti, J. (2007) Mapping substrate selectivity of lipases from thermophilic fungi. *J. Mol. Catal. B: Enzym. 49*, 104–112.
38. van Kampen, M. D., Dekker, N., Egmond, M. R., and Verheij, H. M. (1998) Substrate specificity of *Staphylococcus hyicus* lipase and *Staphylococcus aureus* lipase as studied by in vivo chimeragenesis. *Biochemistry 37*, 3459–3466.
39. van Pée, K. H., Sury, G., and Lingens, F. (1987) Purification and properties of a nonheme bromoperoxidase from *Streptomyces aureofaciens*. *Biol. Chem. Hoppe-Seyler 368*, 1225–1232.
40. Mandrich, L., Merone, L., Pezzullo, M., Cipolla, L., Nicotra, F., Rossi, M., and Manco, G. (2005) Role of the N terminus in enzyme activity, stability and specificity in thermophilic esterases belonging to the HSL family. *J. Mol. Biol. 345*, 501–512.
41. Carrière, F., Thirstrup, K., Hjorth, S., Ferrato, F., Nielsen, P. F., Withers-Martinez, C., Cambillau, C., Boel, E., Thim, L., and Verger, R. (1997) Pancreatic lipase structure-function relationships by domain exchange. *Biochemistry 36*, 239–248.
42. Nixon, A. E., Ostermeier, M., and Benkovic, S. J. (1998) Hybrid enzymes: Manipulating enzyme design. *Trends Biotechnol. 16*, 258–264.
43. Miled, N., Bussetta, C., De caro, A., Rivière, M., Berti, L., and Canaan, S. (2003) Importance of the lid and cap domains for the catalytic activity of gastric lipases. *Comp. Biochem. Physiol., Part B: Biochem. Mol. Biol. 136*, 131–138.
44. Skjøst, M., De Maria, L., Chatterjee, R., Svendsen, A., Patkar, S. A., Østergaard, P. R., and Brask, J. (2009) Understanding the plasticity of the α/β hydrolase fold: Lid swapping on the *Candida antarctica* lipase B results in chimeras with interesing biocatalytic properties. *ChemBioChem 10*, 520–527.
45. Alsop, E., Silver, M., and Livesay, D. R. (2003) Optimized electrostatic surfaces parallel increased thermostability: A structural bioinformatic analysis. *Protein Eng. 16*, 871–874.
46. Ward, T. R. (2008) Artificial enzymes made to order: Combination of computational design and directed evolution. *Angew. Chem., Int. Ed. 47*, 7802–7803.
47. Pleiss, J., Scheib, H., and Schmid, R. D. (2000) The *His gap* motif in microbial lipases: A determinant of stereoselectivity toward triacylglycerols and analogs. *Biochimie 82*, 1043–1052.